processes

*Article*

# Research on Parameter Matching of the Asymmetric Pump Potential Energy Recovery System Based on Multi-Core Parallel Optimization Method

**Lixin Wei [1], Zhiqiang Ning [1,2], Long Quan [3], Aihong Wang [1] and Youshan Gao [1,*]**

1 School of Mechanical Engineering, Taiyuan University of Science and Technology, Taiyuan 030024, China
2 Mechanical and Electronic Engineering Department, Shanxi Institute of Technology, Yangquan 045000, China
3 School of Mechanical Engineering, Taiyuan University of Technology, Taiyuan 030024, China
* Correspondence: 2003011@tyust.edu.cn

**Abstract:** Aiming at the parameters of the different displacements and related components of the variable-displacement asymmetric axial piston pump (VAPP) required by the energy-recovery system of excavator booms of different tonnages, a rapid multi-process parallel optimization method of complex hydraulic products based on a multi-core CPU was proposed for parameter matching. The parameter matching was used to reasonably select relevant parameters so that the excavator's boom energy-recovery and utilization system can improve operational efficiency and energy-saving efficiency under the premise of satisfying the normal working conditions of the working mechanism, and achieving the purpose of serializing VAPP products. A multi-objective optimization model was put forward according to energy-saving efficiency and operational efficiency. First, the accuracy of the acceleration method of the CVODE, a solver for stiff and non-stiff ordinary differential equation (ODE) systems, was verified by a physical prototype test. The results showed that the test and simulation results were in good agreement. A particle swarm optimization algorithm (PSO) was used to optimize the main parameters of the boom energy-recovery system to obtain the appropriate energy-saving efficiency and obtain the VAPP displacement and related component parameters required by the energy-recovery system of excavator booms of different tonnages. The simulation results showed that a motor working condition was necessary in the guaranteed descending stage, and the process of lifting–descending–lifting was completed under the condition that the total time did not exceed a certain value. The energy-saving rates of the 7-ton (7T), 12-ton (12T), 20-ton (20T), and 30-ton (30T) excavator boom energy-recovery systems reached 29.8%, 35.3%, 31.25%, and 27.88%, respectively. In the eight-core CPU workstation under the simulation conditions, compared with the Simulation X platform simulation method, the simulation efficiency of the multi-core CPU parallel method was improved by more than 80 times.

**Keywords:** energy recovery; multi-core CPU; multi-process parallel; serialization products; VAPP



**Citation:** Wei, L.; Ning, Z.; Quan, L.; Wang, A.; Gao, Y. Research on Parameter Matching of the Asymmetric Pump Potential Energy Recovery System Based on Multi-Core Parallel Optimization Method. *Processes* **2022**, *10*, 2298. https://doi.org/10.3390/pr10112298

Academic Editors: Alon Kuperman and Alessandro Lampasi

Received: 5 September 2022
Accepted: 3 November 2022
Published: 5 November 2022



## 1. Introduction

### 1.1. Research Status of Boom Energy-Recovery System for Hydraulic Excavator

The hydraulic excavator is one of the most commonly used pieces of earth-moving machinery, and its high emission and low efficiency have become the focus of current research [1]. The robotic arm of excavation includes a boom, arm, bucket, their respective hydraulic cylinders, and related accessory linkages [2]. The boom system is driven with a differential hydraulic cylinder. The areas of the two chambers of the differential hydraulic cylinder are not equal, and the oil flows required by the chambers are also not equal. For differential hydraulic cylinders controlled by conventional symmetric pumps, additional compensation circuits need be used to balance the flow of the in-cylinder differential, which will complicate the system [3]. When the load or running-speed direction is changed, it is necessary to quickly and accurately switch the oil-filling circuit. That circuit easily leads to air suction and a large pressure impact. Especially in a light load condition, the pressures of the two chambers are close, which degrades the system's stability.

Lodewyks [4] from the Hydraulic Research Institute of RWTH Aachen University, Germany, proposed the loop principle of two variable-displacement hydraulic pumps driven through the shaft and compensated by hydraulic transformers. Zhao et al. [5,6] studied a single-rod hydraulic cylinder system of a hydraulic excavator boom controlled by a double variable-displacement pump driven through the shaft, and used the accumulator to store the falling gravitational potential energy of the boom, which effectively reduced the energy consumption of the system. Erg in Kilic from Turkey studied the control characteristics of a closed-control asymmetric hydraulic cylinder of a dual variable-speed quantitative hydraulic pump, and proposed predicting the pressure of the oil chamber of the variable speed pump-control system based on structured recurrent neural network topology [7]. Dr. Minva of Aalto University, Finland, designed a hydraulic excavator based on a double pump-controlled asymmetric cylinder [8]. However, the cost is higher when two pumps are used to control one actuator.

Zhang et al. [9] proposed a parallel asymmetric axial piston pump, which was used to implement the control of an asymmetric hydraulic cylinder. The valve plate was redesigned based on an ordinary axial piston pump. One side of the oil suction (discharge) window is changed into two independent windows, which are distributed in parallel. The plunger is divided into two different groups on the degree circle, where the two parallel windows are located, so that the plunger is connected with the oil suction (discharge) window. The solution bypasses the auxiliary pump and the auxiliary valve in the hydraulic system. On the other hand, for the reduction in the flow area on one side, it is easy to cause the patency of the oil-absorption process, and limit the maximum speed.

During the working process of conventional excavators, the boom needs to be frequently lifted and lowered, and a large amount of gravitational potential energy is converted into heat energy through the throttle valve [10]. The circuit not only wastes energy, but also causes the system to heat up and reduce the life of components. In a boom system, renewable energy accounts for 72% [11], so research on the energy-saving of hydraulic excavators should focus on the boom system. Recycling and reusing the potential energy of the boom can effectively improve the work efficiency of the excavator.

At present, a boom energy-recovery system can be divided into oil–electric hybrids and oil–liquid hybrids according to different energy-storage components. The energy storage components of an oil–electric hybrid are supercapacitors and batteries, while the energy-storage components of an oil–liquid hybrid are hydraulic accumulators [12]. The oil–electric energy recovery adopts batteries, super-capacitors, etc., as energy-storage elements, and converts the hydraulic energy when the boom is falling into electricity through the hydraulic motor driving the generator to generate electricity for energy recovery [13]. However, the power density of the energy-storage elements is low, and there are many links of energy conversion, so the energy-recovery rate is low. The solution of hydraulic energy recovery adopts a hydraulic accumulator as an energy-storage element. The downward potential energy of the boom is directly recovered and released in the form of hydraulic energy, which has few energy conversion links and high power density, so the hydraulic accumulator is more suitable for boom energy recovery. In addition, the hydraulic accumulator can realize the rapid charging and discharging of the hydraulic oil, and it can also absorb hydraulic shock and eliminate pulsation [14].

A literature review indicates that the system controllability of a multiple composite drive pump or hydraulic valve, which is used to switch system unbalanced flow, is a viable method, although this solution leads to a complex structure, high cost, and a relatively poor operating system. The closed-loop circuit of the pump-controlled cylinder using VAPP could automatically balance the area difference of the asymmetric hydraulic cylinder, which does not require a complex oil-filling circuit [15,16]. However, VAPP is a new-type hydraulic component, which is only trial-produced for 45 mL/r and has not been put into actual serialized production. Therefore, there is a parameter-matching problem in the recovery system of excavator booms driven by VAPP with different tonnages.

### 1.2. Parameter-Matching Method of Boom Energy-Recovery System

In the process of hydraulic system modeling and simulation, multiple parameters need to be adjusted many times to satisfy the design requirement. Lin et al. regarded reducing the installation volume of the accumulator, ensuring the flow matching of the asymmetrical cylinder of the boom and prolonging the service life of the accumulator as constraints [17]. The parameter matching was carried out, and the parameter-matching method of the key components was analyzed. Xiao [18] introduced an asynchronous motor and a supercapacitor into the parallel hybrid structure of the excavator, established an experimental platform for the parallel hybrid excavator, and proposed an engine self-judgment segmented multi-operating point-switching control strategy and engine dynamic operating point. At the same time, aiming at global efficiency optimization, a parameter-matching method based on genetic algorithm was proposed. The optimized power system had the appropriate characteristics of low installed power, high efficiency, and low fuel consumption. In order to improve the oil-saving effect and control performance of a hydraulic hybrid excavator, Tan et al. conducted a parameter-matching simulation study on a 21 T hydraulic hybrid excavator. Wang et al. [19] designed a new type of series hybrid hydraulic excavator with electro-hydraulic composite material for energy storage. The dynamic programming algorithm (DPA) was used to optimize the system parameters, and the effectiveness of the system was verified by experiments. Shen et al. proposed a new hydraulic hybrid excavator with a common pressure rail combined with switched function (HHES) [20]. The optimal matching group was obtained using DPA to match HHES parameters. Lin et al. [21] proposed a parameter-matching method for a parallel hybrid excavator, which improved the system efficiency and reduced the energy-consumption rate through the designed component parameters.

The effectiveness of manually setting parameters relies on the personal experience of software users, and the results obtained are not always optimal. Usually, the simulation only gives the response of the existing system. In order to seek the optimal solution, a new optimization method for parameter matching needs to be proposed in order to be combined with the simulation module of the hydraulic system.

By analyzing and summarizing the above literature, the current problems in the optimization design and human–computer interaction of hydraulic simulation software are as follows:

(1) When optimizing parameters of current hydraulic products, professional simulation software needs to be installed in advance, and could not run independently in a Windows operating system without a simulation platform.
(2) When optimizing the parameters of the simulation software platform, the optimization is mainly carried out by serial iteration. The professional simulation platform has high demand for memory and CPU, and it is very slow for a computer to carry out two simulation platforms at the same time. Therefore, a parallel simulation based on simulation-platform software demands higher performance equipment, and it is inconvenient to carry.
(3) The human–machine interaction interface is unfriendly. Manual input is required to change the initial parameter value, and manual parameter modification is cumbersome and involves a lot of repetitive work.

Therefore, a rapid multi-process parallel optimization method for complex hydraulic products based on a multi-core CPU was proposed. The proposed optimization method adopts the CVODE solver, which can speed up the simulation and realize the separation from the simulation software platform. The CVODE external solver is an external solver for rigid and non-rigid models and simulation types that do not have many interruptions. Since the model algorithm is based on compilation, applying this solver to complex models is faster. The multi-core CPU acceleration method assigns a process to each population individual and performs iterative calculations independently, according to the optimization-algorithm process. The individuals are solved independently in parallel and do not interfere with each other. The multi-core parallel optimization method was applied to the serial development of VAPP products and the parameter optimization of related components of the boom energy-recovery system.

In summary, the main contributions are as follows.

(1) In this article, VAPP is used to drive the excavator boom, which can solve the flow mismatch problem of the boom and reduce the complexity of the hydraulic system.
(2) A rapid multi-process parallel optimization method for complex hydraulic products based on a multi-core CPU is proposed to solve the optimization parameter-matching problem.
(3) The above optimization method is applied to the energy-recovery system of excavating booms of different tonnages to obtain the appropriate energy-saving rate of boom system, and the recommended values of VAPP-related design parameters for different displacement are given. The remainder of this paper is organized as follows: In Section 2, the working principles and displacement design of VAPP are described and analyzed. In Section 3, the energy-recovery system parameter matching is presented and analyzed. A parallel parameter-matching method based on a multi-core CPU are studied in Section 4. Finally, the conclusions are presented in Section 5.

## 2. Working Principle and Displacement Design of VAPP

Variable displacement asymmetric axial piston pumps are used in hydraulic circuits [22]. The working principle of their variable displacement is to adjust the inclination angle of the swashplate using the control mechanism, so that it changes the flow rate of the pump outlet, and then obtains different ascending speeds under the same load condition.

The schematic diagram of the VAPP-driven hydraulic cylinder and potential energy recovery is shown in Figure 1. As the main component of potential energy recovery, VAPP is different from ordinary two-port pumps. It has three distribution windows. An unloading groove is added to the distribution window, which can effectively improve the overall characteristics of VAPP.

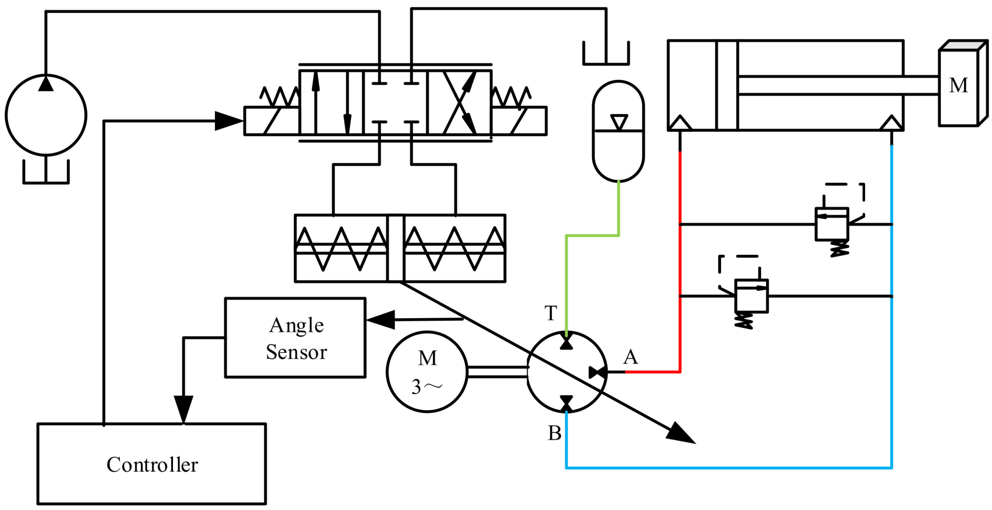


**Figure 1.** Schematic of differential cylinder driven by VAPP and energy recovery.

It can directly change the inclination of the swashplate so that the distribution windows A and B can obtain different flows to drive the movement of the hydraulic cylinder without other auxiliary components. The distribution window A is connected to the rodless chambers of the hydraulic cylinder, and the distribution windows B and T are connected to the rod chamber and the accumulator of the hydraulic cylinder, respectively. Theoretically, the flow of distribution window A is equal to the sum of the flow of distribution windows B and T.

In the beginning, the load is at the lowest position. The motor drives the VAPP to work, and the VAPP is in pump's condition at this time. The hydraulic oil enters the rodless chamber of the hydraulic cylinder through the distribution window A to drive the load to lift.

The swash-plate angle of the VAPP is changed by the control mechanism, and the VAPP is in the working state of the hydraulic motor at this time. Hydraulic oil enters the connecting-rod chamber of the cylinder through the distribution window B. At the same time, part of the hydraulic oil is stored by the accumulator through the distribution window T.

When the load rises for the second time, the energy stored in the accumulator is released to speed up the rise of the load and reduce the work performed by the motor, thereby achieving potential energy recovery and utilization. In this VAPP system, the throttling loss is reduced, and the integration of drive and energy recovery can be realized.

The distribution window is shown in Figure 2. It can be seen from the figure that there are three transition zones in the series asymmetric flow distribution plate, namely the top dead-center TDC, the nominal dead-center NDC and the bottom dead-center BDC [23].

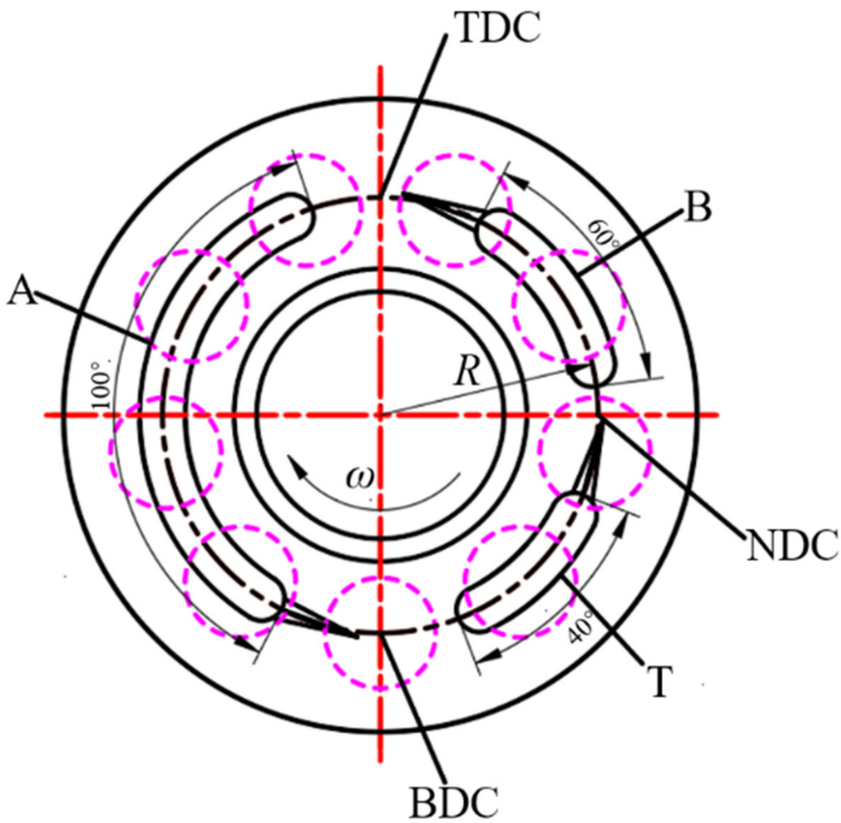


**Figure 2.** Schematic diagram of the distribution window.

The VAPP belongs to the conical cylinder axial piston pump in structure, and its structure diagram is shown in Figure 3. Unlike the structure in which the plungers in the cylindrical plunger pump are evenly distributed along the cylindrical surface, the plunger axis of the conical cylinder axial piston pump forms a certain angle with the cylinder axis and is distributed along the conical surface. Although this renders the movement trajectory of the plunger more complex and increases the difficulty of solving the equation of motion at the same speed, the linear velocity of the pump distribution surface will be relatively low, which enables it to operate at a higher speed. Therefore, a larger displacement of the piston pump can be obtained under the same conditions.

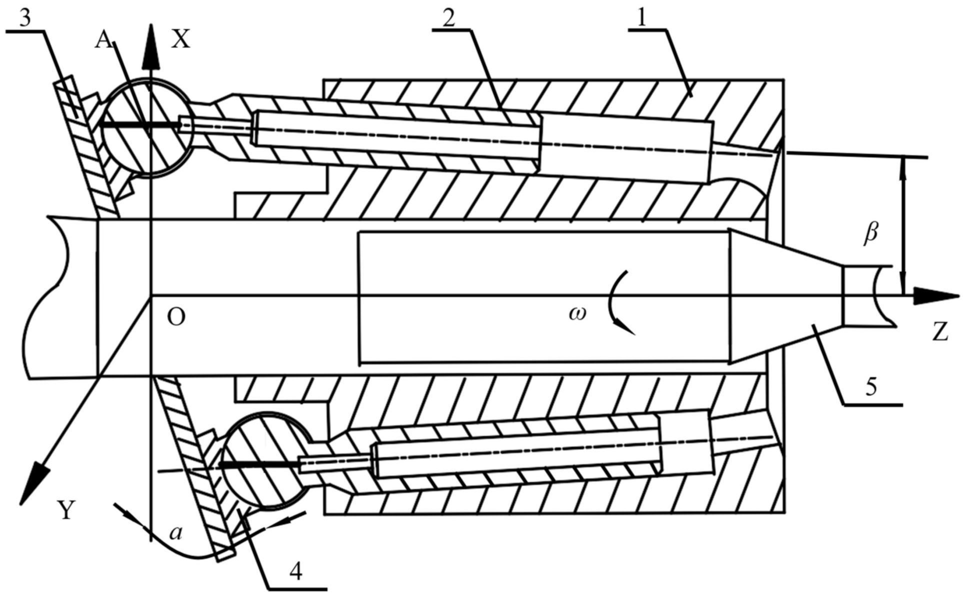


**Figure 3.** Conical piston-pump structure diagram: 1. Cylinder block, 2. Plunger, 3. Swashplate, 4. Piston shoes, 5. Spindle.

When the conical piston pump moves in the direction of rotation as shown in Figure 3, the kinematics of the plunger are analyzed at the top dead center, A. During the movement of the plunger, on the one hand, it rotates with the cylinder block. On the other hand, it moves back and forth in the cylinder block. According to the actual movement trajectory of the plunger head, the spatial coordinate system as shown in Figure 4 is constructed from the spatial position relationship, it can be concluded that the movement trajectory of the plunger head is the intersection point between the cone of the plunger axis and the plane of the swashplate.

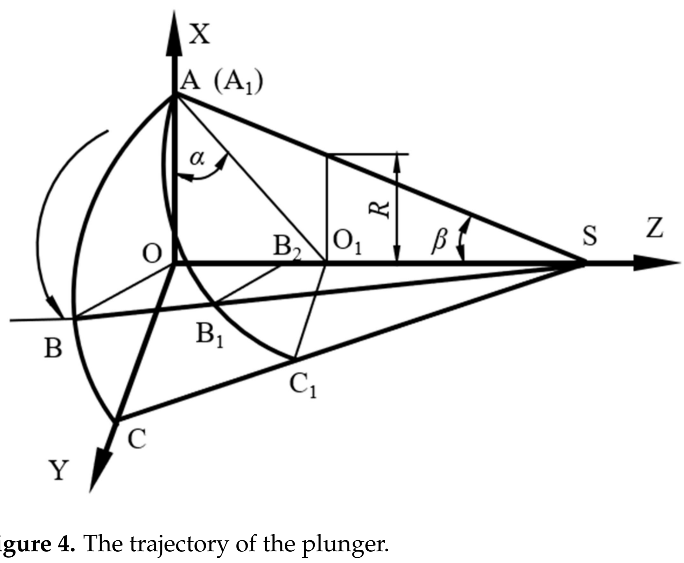


**Figure 4.** The trajectory of the plunger.

In Figure 4, point $S$ is the apex of the conical surface where the axis of the plunger is located. $OS$ is the axis of the main shaft of the cylinder. The planes $OAC$ and $O_1A_1C_1$ are the bottom surface of the conical surface where the axis of the plunger and swashplate are located, respectively. The arc $A_1B_1C_1$ is the movement trajectory of the plunger head originally located at the top dead center, $A$. The length of the line segment $OA$ represents the distance from the plunger head at $A$ to the cylinder axis when the swashplate inclination angle is $\alpha$, and $R$ represents the distance from the plunger head at the top dead center to the cylinder axis when $\alpha = 0$. $B_1$ represents the position of the plunger head when the cylinder rotates through the angle $\phi$, and $B_2$ is the projection of point $B_1$ on the $z$-axis.

$$x(\phi) = B_1 B_2 \cos\phi \tag{1}$$

$$y(\phi) = B_l B_2 \sin\phi \tag{2}$$

$$z(\phi) = OB_2 = OS - SB_2 = \frac{OA}{\tan\beta} - \frac{B_1 B_2}{\tan\beta} \tag{3}$$

In Figure 4, point $P_1$ is created by connecting point $O_1$ and point $B_1$ and extending it. The plane view of the axis of the plunger is shown in Figure 5a. In the $xOy$ plane, the vertical line of the $x$-axis passing through the top dead center, $A$, and the extension line of $OB$ intersect at the point $P_2$. As shown in Figure 5b, it is a schematic diagram of the intersection of the vertical line of the $x$-axis passing through the point, $A$, and the moving plane. According to the spatial relationship, the point $P_2$ and the point $P_1$ are coincident in spatial geometric relationship.

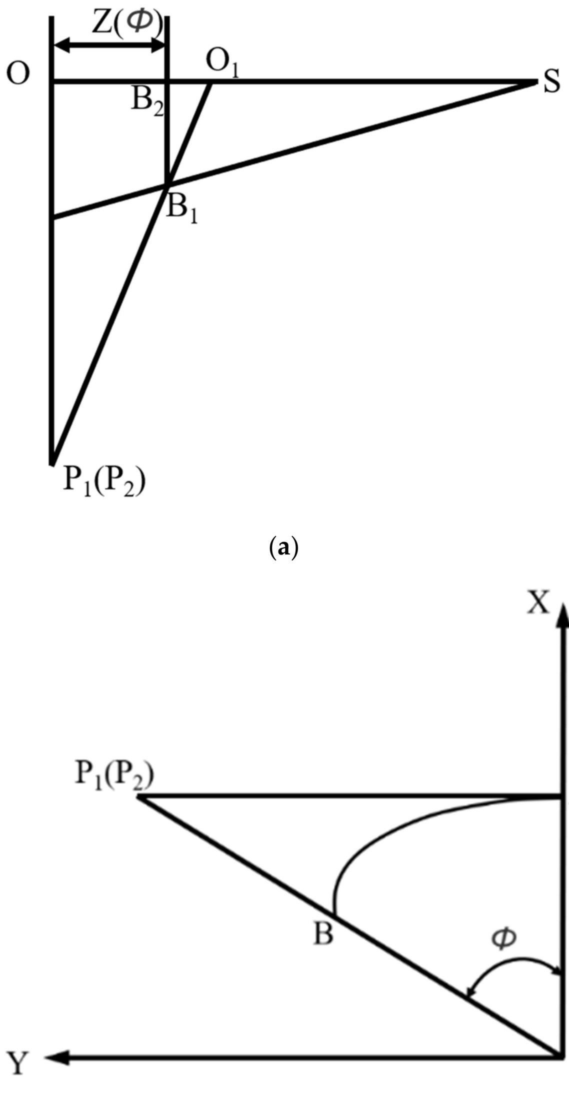


**Figure 5.** Auxiliary schematic diagram of plunger ball head $B_1$ (**a**) The plane of the plunger axis (**b**) The intersection of the vertical line and the moving plane.

From the similarity of triangles, the following formula can be obtained:

$$\tan \angle O_1 B_1 B_2 = \tan \angle O P_1 O_1 = \cos\phi \tan\alpha \tag{4}$$

According to Figure 4, this formula can be obtained:

$$OO_1 = OA \tan\alpha \tag{5}$$

According to Figure 5a, this formula can be obtained:

$$B_1 B_2 \tan \angle O_1 B_1 B_2 = OO_1 - z(\phi) \tag{6}$$

Substituting Equations (4) and (5) into Equation (6), this formula can be obtained:

$$B_1 B_2 \cos\phi \tan\alpha = OA \tan\alpha - z(\phi) \tag{7}$$

Simultaneously, Formulas (3) and (7) are achieved:

$$B_1 B_2 = \frac{OA \cos(\phi + \beta)}{\cos\phi \cos\beta (1 - \tan\alpha \tan\beta \cos\phi)} \tag{8}$$

According to Figure 4, it can be known from the geometric relationship:

$$OA = R\frac{\cos\alpha \cos\beta}{\cos(\phi + \beta)} \tag{9}$$

Substituting Equation (9) into Equation (8) produces:

$$B_1 B_2 = \frac{R}{(1 - \tan\alpha \tan\beta \cos\phi)} \tag{10}$$

Incorporating Equation (10) into Equations (1)–(3) produces:

$$\begin{cases} x(\phi) = R\frac{\cos\phi}{(1-\tan\alpha\tan\beta\cos\phi)} \\ y(\phi) = R\frac{\sin\phi}{(1-\tan\alpha\tan\beta\cos\phi)} \\ z(\phi) = R\frac{\sin\alpha\cos\beta(1-\cos\phi)}{(1-\tan\alpha\tan\beta\cos\phi)\cos(\alpha+\beta)} \end{cases} \tag{11}$$

The displacement equation of the plunger in the conical cylinder is:

$$S(\phi) = \frac{z(\phi)}{\cos\beta} = \frac{R\sin\alpha(1 - \cos\phi)}{(1 - \tan\alpha\tan\beta\cos\phi)\cos(\alpha + \beta)} \tag{12}$$

The relationship between the speed of the plunger relative to the cylinder is:

$$v = \frac{dS(\phi)}{dt} = \frac{dS(\omega t)}{dt} = R\omega\frac{\sin\alpha\sin\phi(1 - \tan\alpha\tan\beta)}{\cos(\alpha + \beta)(1 - \tan\alpha\tan\beta\cos\phi)^2} \tag{13}$$

where: $\alpha$ is the inclination angle of the swashplate. $\phi$ and $\omega$ are the rotation angle and angular velocity of the cylinder, respectively.

From the derived kinematic Equation (12) of the plunger of the conical plunger pump, the maximum displacement of the plunger in the cylinder is:

$$S_{max} = S(\phi)|_{\phi=\pi} = \frac{2R\sin\alpha}{(1 + \tan\alpha\tan\beta)\cos(\alpha + \beta)} \tag{14}$$

The theoretical displacement $q_T$ of the conical piston pump can be obtained as:

$$q_T = \frac{\pi}{4} d^2 Z S_{max} = \frac{RZ\pi \sin\alpha d^2}{2(1+\tan\alpha\tan\beta)\cos(\alpha+\beta)} \tag{15}$$

where: $d$ is diameter and $Z$ is the number of plungers, respectively.

Therefore, the instantaneous theoretical flow of the conical plunger pump can be further solved:

$$\begin{aligned} Q(T) &= \sum_n^{i=1} Av_i = \sum_n^{i=1} \frac{AR\omega \sin\alpha(1-\tan\alpha\tan\beta)\sin\phi_i}{\cos(\alpha+\beta)(1-\tan\alpha\tan\beta\cos\phi_i)^2} \\ &= K\sum_n^{i=1} \frac{\sin\phi_i}{(1-\tan\alpha\tan\beta\cos\phi_i)^2} \end{aligned} \tag{16}$$

where: $K = \frac{AR\omega\sin\alpha(1-\tan\alpha\tan\beta)}{\cos(\alpha+\beta)}$

$A$ is the cross-sectional area of the plunger; $n$ is the number of plungers in the oil-discharge area at a certain time. Since the pump has nine plungers in total, which is an odd number, $n = (Z \pm 1)/2; \phi = \phi + \theta(i-1)$, where $\theta = 2\pi/Z$ represents the angular distance between plunger and plunger.

## 3. Match VAPP Energy-Recovery System Parameters

The optimization problem refers to finding the optimal solution or parameter value among many solutions or parameter values under certain conditions so that some functional indicators of the system can reach the maximum or minimum value. In this article, parameter matching is the crucial link between the VAPP-controlled differential cylinder and potential energy recovery.

### *3.1. Experimental Verification of Simulation Model*

Using ITI-SimulationX software to build a simulation model of a VAPP-controlled differential cylinder and an integrated hydraulic circuit for kinetic energy recovery. The model is as shown in Figure 6.

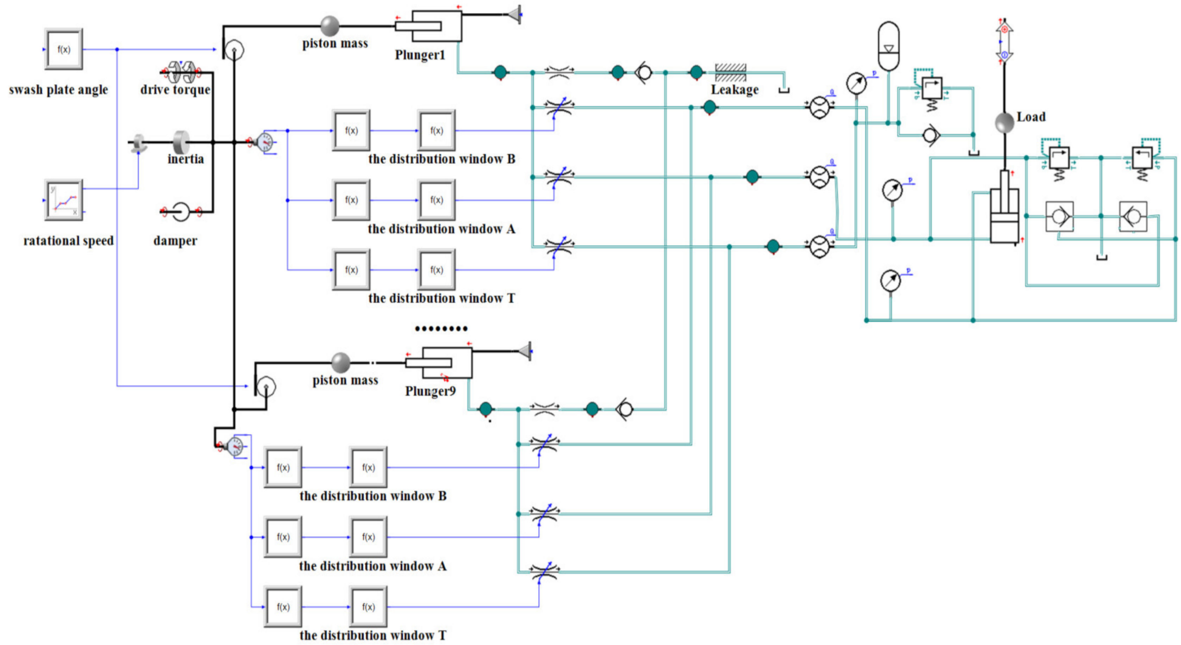


**Figure 6.** Simulation model of the proposed system.

In actual work, the load fluctuation of the operating mechanism is relatively large, and the energy-recovery efficiency is also greatly affected by the actual working conditions. To facilitate analysis and comparison, the typical working conditions of the excavator boom were established, and the potential energy of the VAPP-controlled differential cylinder and the integrated hydraulic circuit of kinetic energy recovery were analyzed. The key parameters of the proposed system are shown in Table 1.

**Table 1.** Parameters used in simulations.

| Model Parameters | Parameter Value | Unit |
|---|---|---|
| Plunger diameter | 17 | mm |
| Number of plungers | 9 | / |
| Rated displacement | 45 | ml/r |
| Piston stroke | 22.2 | mm |
| Distribution-groove distribution-circle diameter | 33.5 | mm |
| The maximum inclination of swashplate | 18.3 | ° |
| Plunger distribution-circle radius | 33.5 | mm |
| Total stroke of hydraulic cylinder | 750 | mm |
| Hydraulic cylinder diameter | 63 | mm |
| Hydraulic cylinder-rod diameter | 45 | mm |
| Adjustable relief valve | YF-L20H | 0–10 MPa |
| S type check valve | S6A | 0.05 MPa |

In this paper, the simulation analysis results of the potential energy-recovery system of the VAPP-controlled differential cylinder are verified by a physical prototype test. The experiment bench consists of the VAPP, differential cylinder, accumulator, variable frequency motor, and control system. During the experiment [15], since it was impossible to observe whether the hydraulic cylinder has risen or fallen to the limit position, it was necessary to use a displacement sensor to complete it, as shown in Figure 7. By observing the data measured by the displacement sensor, the displacement of the load can be recorded, and it can also provide a basis for DSpace to control the electro-hydraulic servo valve of the variable mechanism on the VAPP.

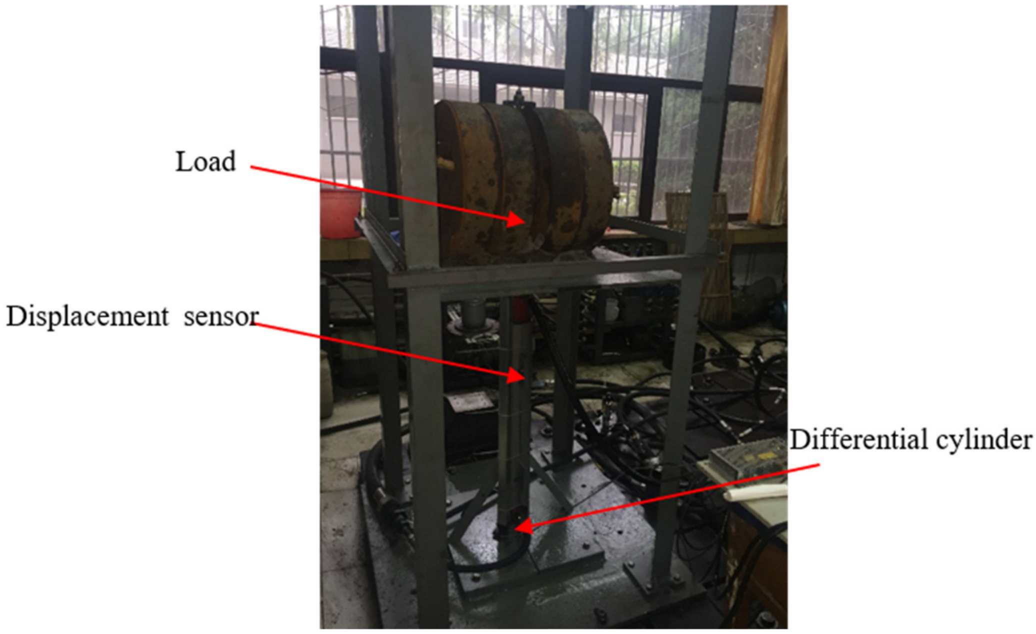


(**a**)

**Figure 7.** *Cont*.


(**b**)

**Figure 7.** Main components of the test bench (**a**,**b**).

During the test, the speed and direction of rotation of the motor are set unchanged. When working, the VAPP is driven by the motor, and DSpace sets the electro-hydraulic servo-valve signal to control the swash-plate inclination, as shown in Figure 8.

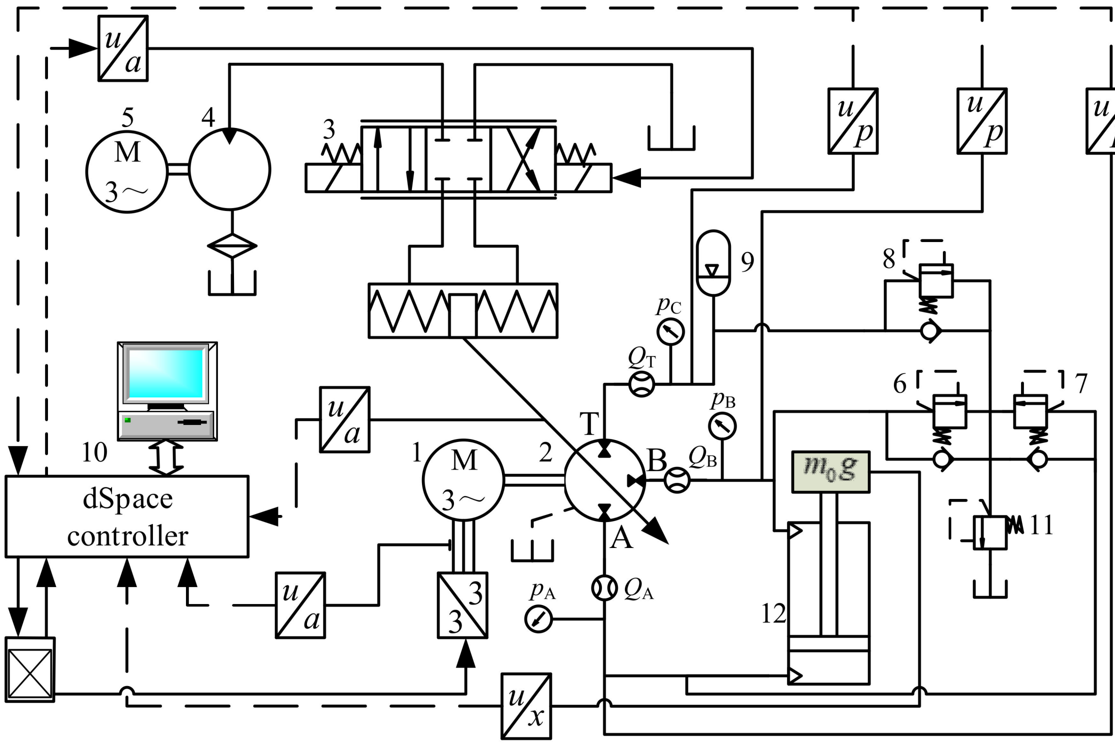


**Figure 8.** Principle of the test rig.

During the test, the load was set at 440 kg, the motor speed was 1000 rpm, and the inclination angle of the VAPP swashplate was 5°. Sorting out the measured data of the load-displacement by the displacement sensor during the experiment, the comparison between the experiment and simulation is shown in Figure 9. It can be seen from the figure that during the test, the swash-plate-angle control system fluctuated, which may have been caused by the inability of the motor to output a constant speed. The fluctuation was more obvious especially when the inclination angle of the swashplate of the VAPP changed suddenly.

$$E_{mce} = \int p_A Q_A dt \tag{17}$$

where: $p_A$ is the pressure at port A. $Q_A$ is the flow at port A.

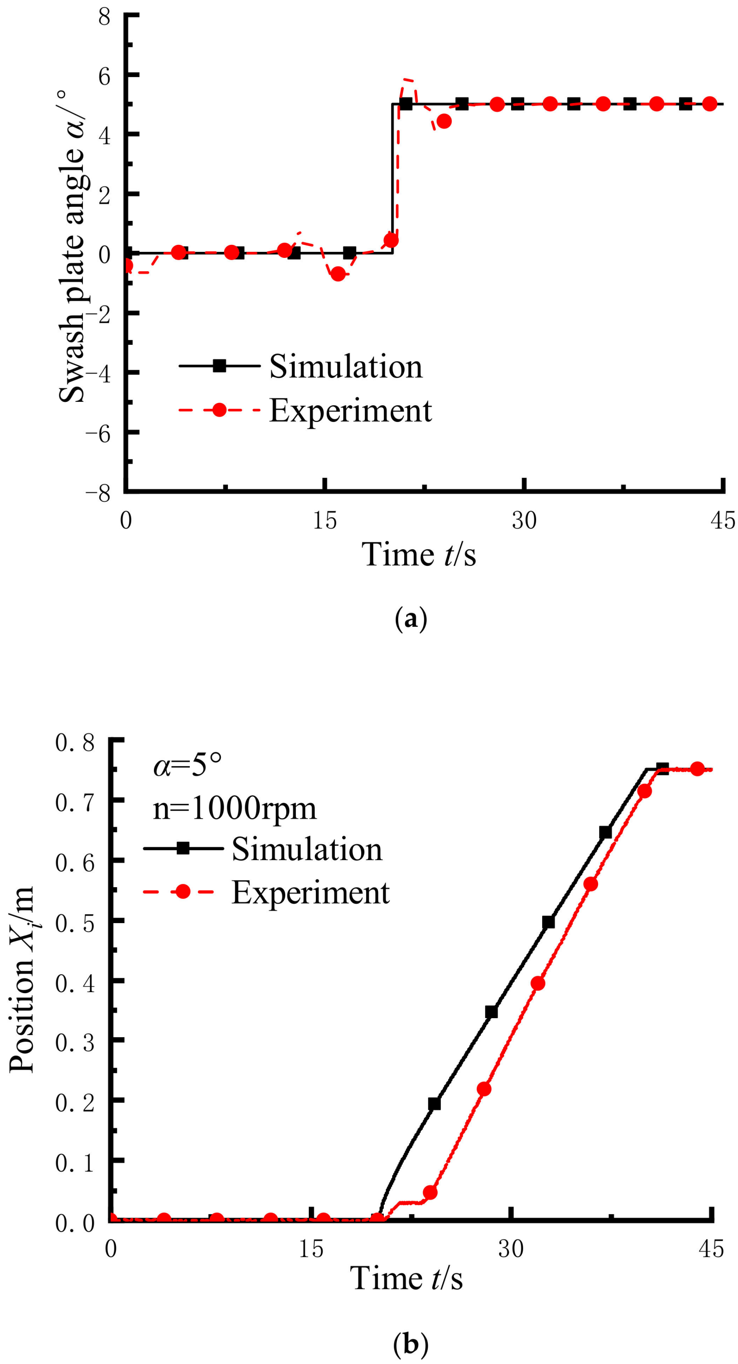


**Figure 9.** (**a**) The change in inclination angle with time (**b**) The change in load position with time.

Formula (17) is used to calculate the energy consumed by the motor. Under the same conditions, the simulated and experimental motor energy-consumption figures are shown in Figure 10.

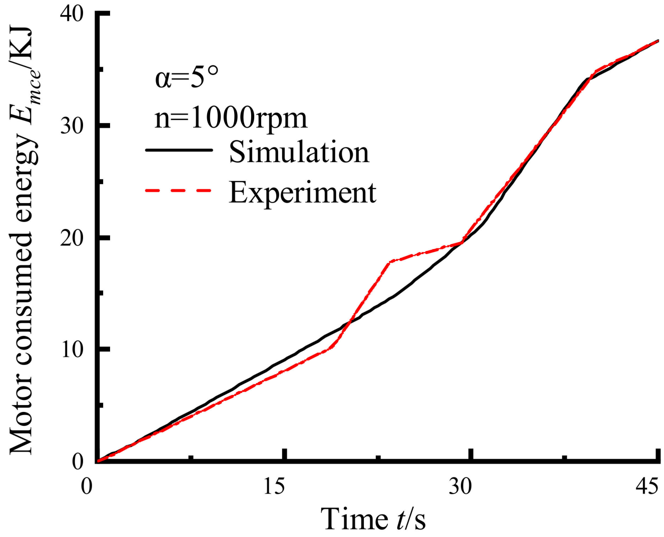


**Figure 10.** The change in energy consumption with time.

By comparing the experimental and simulation results, it is found that the simulation can well represent the process required by the experiment.

*3.2. VAPP Potential Energy-Recovery System Parameter Matching*

There are many factors affecting the performance of the potential energy-recovery system. The displacement of VAPP, motor speed, initial charging pressure and volume of the accumulator, the angle of the swashplate in the descending stage, and the load weight will affect the potential energy-recovery efficiency and boom-operation performance in the descending stage. From the perspective of its engineering application, the potential energy-recovery system requires an operation speed that is as rapid as possible, high-energy-recovery efficiency, and a small VAPP displacement, but it is difficult to take these all into account at the same time. Thus, it is necessary to balance them by parameter matching. A force diagram of the hydraulic excavator boom was created, as shown in Figure 11. The load characteristics of the boom system were analyzed by Xia et al. [24].

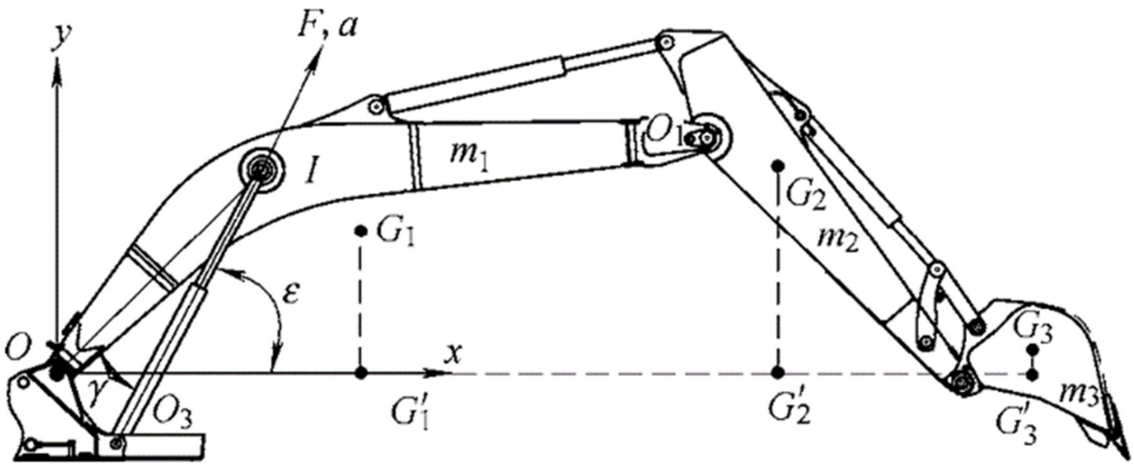


**Figure 11.** Force diagram of the hydraulic excavator boom.

The running trajectory of the excavator working device is the rotational motion around the hinge point $O$, and its equivalent moment of inertia is:

$$J = J_1 + J_2 + J_3 + m_1 L_{oG1}^2 + m_2 L_{oG2}^2 + m_3 L_{oG3}^2 \quad (18)$$

In Formula (18), $m_1$, $m_2$, and $m_3$ are the masses of the boom, arm, and bucket, respectively. $J_1$, $J_2$, and $J_3$ are the moments of inertia of the boom, arm, and bucket relative to their center of gravity. $L_{\mathrm{oG1}}$, $L_{\mathrm{oG2}}$, $L_{\mathrm{oG3}}$ is the distance from the center of gravity of the boom, the arm, and the bucket to the hinge point $O$, respectively.

The resultant force of the boom at the hinge point $I$ is $F$, and the torque balance equation at the hinge point $O$ is:

$$FL_{\mathrm{OI}} \sin\gamma = Ja \sin\gamma / L_{\mathrm{OI}} \tag{19}$$

In Formula (19), $L_{\mathrm{OI}}$ is the distance from the hinge point $O$ to the hinge point $I$, $a$ is the acceleration of the boom at the hinge point $I$ along the direction of the hydraulic cylinder, $a \sin\gamma / L_{\mathrm{OI}}$ is the angular acceleration of the boom around the hinge point $O$, and $J$ is the equivalent moment of inertia of boom, arm, bucket, and load about hinge point $O$.

According to Newton's second law:

$$F = ma \tag{20}$$

It can be known from the simultaneous Equations (19) and (20) that the equivalent mass of the hydraulic excavator working device at the hinge point $I$ is:

$$m = \frac{J}{L_{\mathrm{OI}}^2} \tag{21}$$

The simulation parameters of accumulator volume, the initial pressure of accumulator, and the motor speed are set to 10 L, 2 MPa, and 2000 rpm, respectively. The minimum equivalent load mass of 7T excavator is calculated when the arm cylinder and the bucket cylinder are extending. In this condition, the equivalent load mass calculated according to Formula (21) is 2500 kg, and the swashplate inclination in the descending stage is controlled by $-5°$ through the control system. The simulation results of the load position are shown in Figure 12. When the displacement of the VAPP increases, the response of the load becomes rapider.

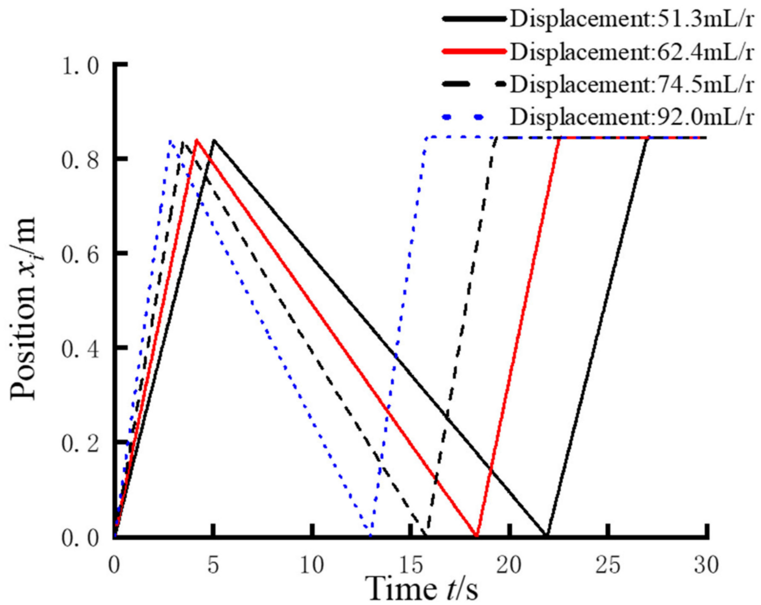


**Figure 12.** Load position with different displacement of VAPP.

Figure 13 shows the simulation results of the motor's energy consumption changing with the displacement of the VAPP. When the displacement of VAPP increases, the total energy consumed increases gradually.

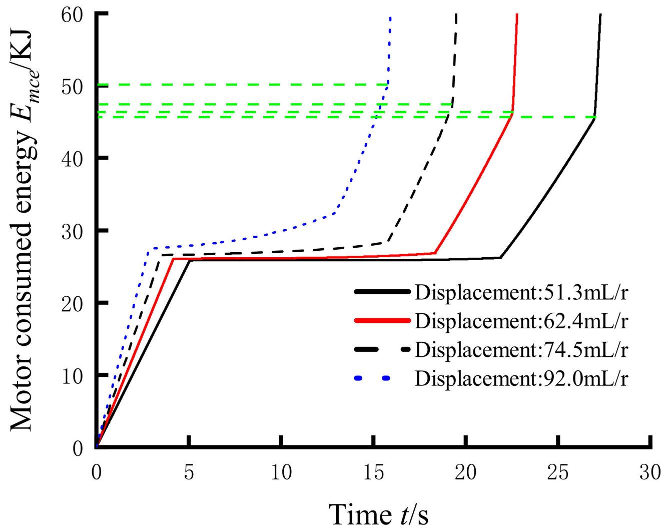


**Figure 13.** Energy consumption with different displacement of VAPP.

The energy consumption and operating efficiency of the first lifting and the second lifting of the load under different displacements of VAPP are shown in Table 2. From the table, it can be seen that due to the recovery and reuse of potential energy, the motor can reduce energy consumption, $E$. The energy consumed to complete the first lift is $E_{1up}$; the energy consumed to complete the first descent is $E_{down}$. The energy consumed to complete the second lift is $E_{2up}$; the energy consumed to complete the lifting–lowering–re-lifting is $E_{sum}$, and the energy-saving rate is $\eta$. The gravitational potential energy of the equivalent mass is $E_m$.

$$E_m = mgh \tag{22}$$

**Table 2.** Energy-consumption comparison.

| Displacement/mL$r^{-1}$ | $E_{1up}$/KJ | $E_{down}$/KJ | $E_{2up}$/KJ | Total Lift-Descent-Lift Time/s | Descent Time/s | Energy Saving Rate $\eta$ |
|---|---|---|---|---|---|---|
| 51.3 | 25.8 | 0.410 | 19.0 | 26.9 | 16.85 | 30.9% |
| 62.4 | 26.0 | 0.801 | 19.1 | 22.5 | 14.14 | 29.8% |
| 74.5 | 26.4 | 1.9 | 18.6 | 19.2 | 12.3 | 28.3% |
| 92.0 | 27.5 | 4.9 | 17.5 | 15.7 | 10.1 | 24.5% |

In Formula (22), $m$ is the equivalent mass, $g$ is the acceleration of gravity, and $h$ is the lifting height.

$$\eta = \frac{2 * E_{1up} - E_{sum}}{E_m} \tag{23}$$

The simulation parameters of the accumulator volume, the initial charging pressure of the accumulator, the displacement of VAPP, the angle of the swashplate in the descending stage, and the equivalent mass of load are set to 10 L, 2 MPa, 62.4 mL/r, 7°, and 2500 kg, respectively. Under the above simulation conditions, the speed of the motor is changed for the simulation. Figure 14 shows the motor energy consumption with different speeds. When the speed of the motor increases, the energy consumption of the motor increases gradually.

The simulation parameters of the accumulator volume, the initial charging pressure of the accumulator, the displacement of VAPP, the speed of motor, and the equivalent mass of load were set 10 L, 2 MPa, 62.4 mL/r, 2000 rpm and 2500 kg, respectively. Under the above simulation conditions, the angle of the swashplate in the descending stage was changed for simulation. Figure 15 shows the change in load position and energy consumption with different swashplate inclinations. It can be seen from Figure 15 that with the swashplate inclination increasing in the descending stage, the response of the load becomes more rapid. However, when the swashplate inclination increases in descending, the motor drags the load, which is not conducive to energy recovery. The energy consumption of a swashplate inclination of 18° in the descending stage is more than that for a swashplate inclination of 5°.

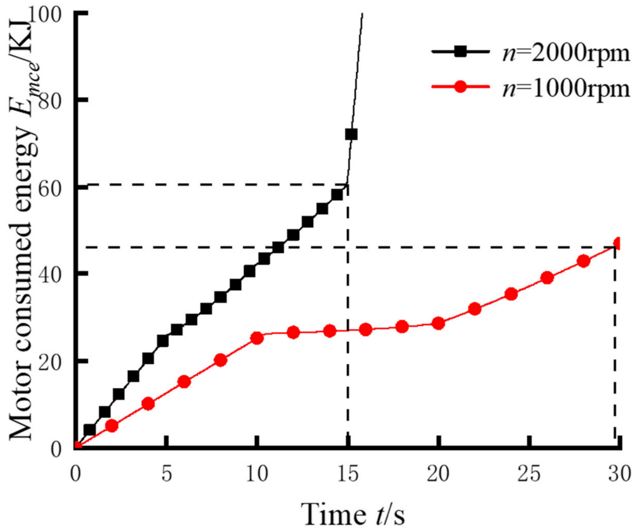


**Figure 14.** Energy consumption with different speeds.

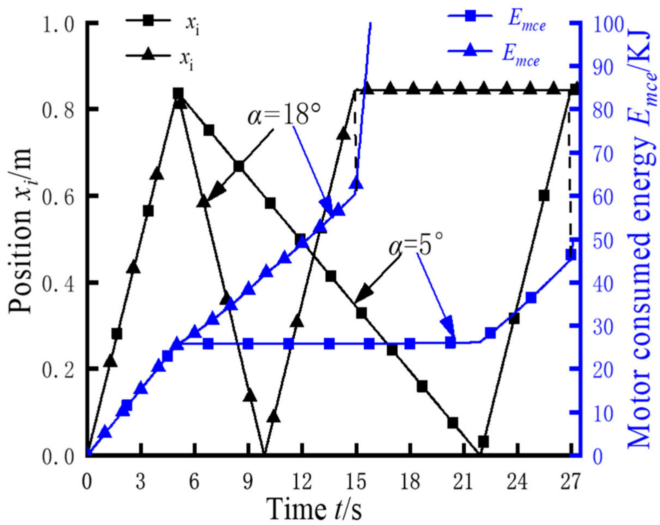


**Figure 15.** Load position and motor energy consumption under different swashplate inclinations in descending stage.

The simulation parameters of the angle of the swashplate in the descending stage, the speed of the motor, the displacement of VAPP, and the equivalent mass of load are set to 7°, 2000 rpm, 62.4 mL/r, and 2500 kg, respectively. Under the above simulation conditions, the accumulator volume and the initial charging pressure of the accumulator are changed for the simulation. Figure 16 shows that when the accumulator volume is the same and the initial charging pressure of the accumulator increases, the energy consumption of the motor increases gradually. When the initial charging pressure of the accumulator is the same and the accumulator volume of the accumulator increases, the energy consumption of the motor descends gradually, but the response of the load becomes slower.

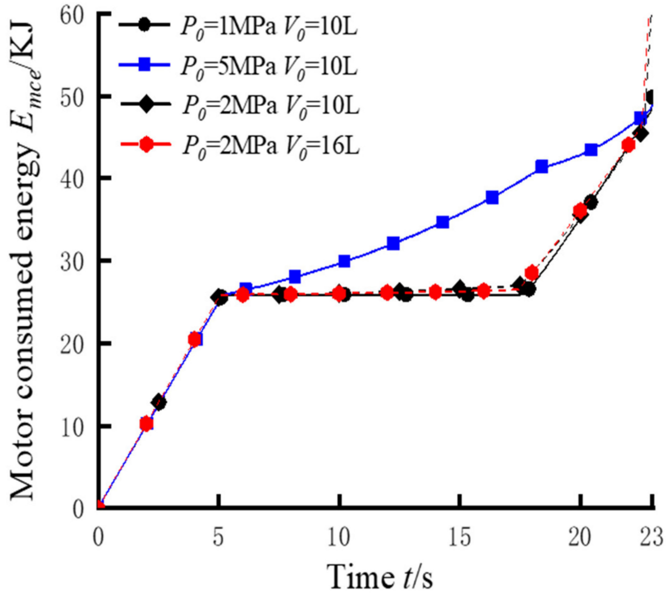


**Figure 16.** Motor energy consumption under different initial charging pressures $P_0$ of accumulator and the volumes $V_0$ of accumulator.

The simulation parameters of the accumulator volume, the initial charging pressure of the accumulator, the displacement of VAPP, the speed of motor, and the angle of swashplate in the descending stage are set 10 L, 2 MPa, 62.4 mL/r, 2000 rpm and 7°, respectively. Under the above simulation conditions, the equivalent mass of load is changed for simulation. Figure 17 shows that when the equivalent load mass is 5000 kg, the energy consumption in the descending stage is lower than 2500 kg. This is because the motor's working conditions in the descending stage are related to the load. The larger the load, the easier it is to form a motor. The working condition, that is, the load that "drags" the motor to rotate, is conducive to the conversion of potential energy into accumulator energy.

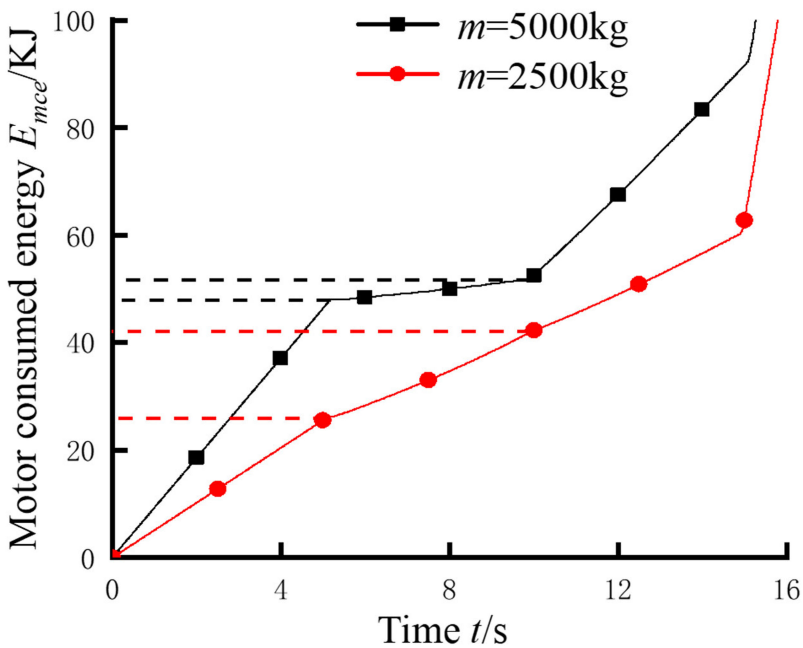


**Figure 17.** Motor energy consumption under different equivalent load mass $m$.

## 4. Parallel Parameter-Matching Method Based on Multi-Core CPU

### *4.1. Rapid Parallel Optimization Method Framework for VAPP Products Based on Multi-Core CPU*

The main principle of the rapid parallel optimization method for complex hydraulic products with a multi-core CPU is to dynamically tune the simulation parameters for the CVODE simulation program based on the PSO. The CVODE solver can improve the simulation speed. The CVODE executable simulation program is regarded as the swarm particles of a swarm-intelligence algorithm. Each particle (CVODE executable program) is assigned to different design parameters, and the parameterization process is realized by writing the parameter file [25].

The product performance parameters can be extracted from the output files generated by the COVDE executable program. The fitness value of the swarm particles can be calculated; at the same time, it can be judged whether the product performance constraints are met. Different from the traditional serial optimization simulation method, each COVDE executable program is a DOS program, which can be started and run through the ShellExecute function, and a process is automatically generated. If multiple DOS programs are started, the process allocation rights belong to the operating system, and there is no need for human intervention.

Running a simulation of multiple DOS processes can make full use of multi-core processors, and data interaction with the module can be conducted until the iteration-termination condition is met. Given the poor human–computer interaction of professional hydraulic simulation software, the visual interaction module is also a necessary part. The mainframe structure of the multi-core CPU parallel optimization method is shown in Figure 18.

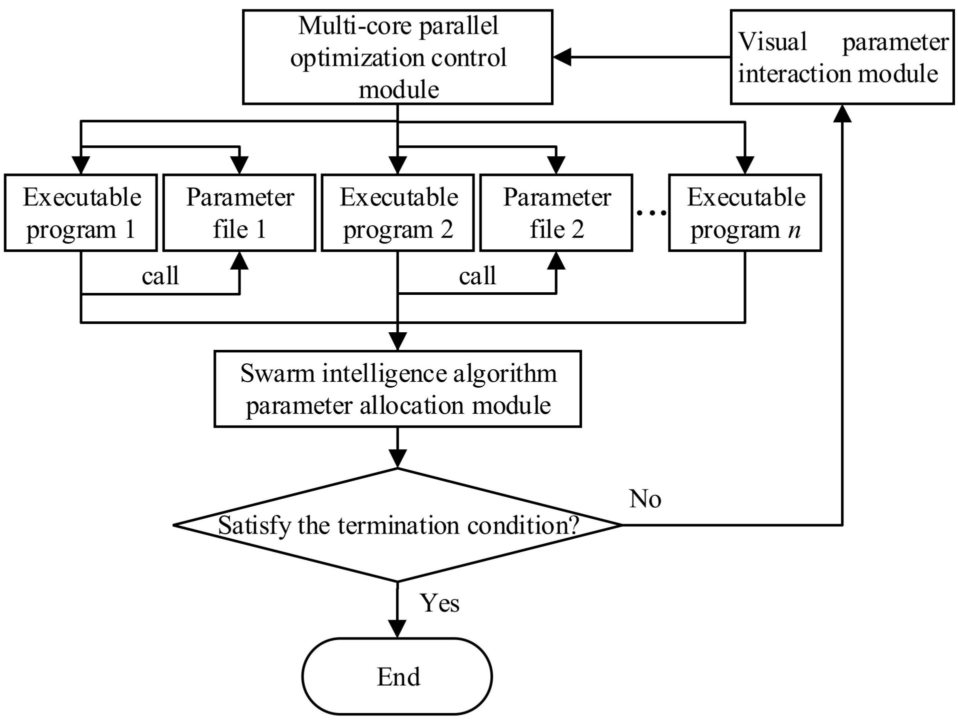


**Figure 18.** The frame of parallelism optimization is based on swarm intelligence.

### *4.2. Processing of PSO Multi-Objective Functions and Constraints in Parallelism Simulation*

Multi-objective optimization is when multiple objectives need to be achieved and, due to the inherent conflict between objectives, the optimization of one objective is at the expense of the degradation of other objectives, so it is difficult to obtain a unique optimal solution; instead, it is made by coordinating and compromising to render the overall goal as optimal as possible. According to the linear combination method, multiple objective functions form a comprehensive objective function [26].

Through the above comparative simulation analysis, it can be seen that the equivalent mass of load, initial charging pressure $P_0$, and volume of the accumulator $V_0$, the angle of swashplate in the descending stage, the displacement of VAPP, and the motor speed will all have an impact on the operation efficiency and energy consumption. The larger the displacement, the higher the working efficiency, but it is not conducive to the potential energy-recovery system to form a motor condition in the descending stage. If the swashplate inclination is too large in the descending stage, it may affect the energy recovery, but if it is too small, the load will descend too slowly. Therefore, the parameter matching of the asymmetric pump potential energy-recovery system should take into account low energy consumption and high operation efficiency. The multi-objective optimization method provides an effective way of parameter matching the asymmetric pump potential energy-recovery system.

Design variables: asymmetric pump displacement $V_P$, accumulator charging pressure $P_{AC}$, initial volume $V_{AC}$ and the swashplate inclination $\beta$ in the descending stage.

Objective function 1: lifting–lowering–re-lifting total energy consumption $E \rightarrow min$.

Objective function 2: the swashplate inclination $\beta$ in the descending stage$\rightarrow max$.

Convert each sub-objective function to take a value in the range of 0 to 1.

$$f_E = \frac{E - E_{min}}{E_{max} - E_{min}} \tag{24}$$

$$f_\beta = \frac{\beta - \beta_{min}}{\beta_{max} - \beta_{min}} \tag{25}$$

In Formulas (24) and (25), the energy-consumption lower bound value of the total energy-consumption objective function is $E_{min}$ and the upper bound value $E_{max}$, the angle lower bound value is $\beta_{min}$ and the upper bound value of the swashplate-angle objective function is $\beta_{max}$.

The objective function of the asymmetric pump potential-energy-recovery system:

$$f = W_1 f_E - W_2 f_\beta \rightarrow \min \tag{26}$$

In Formula (26), $W_1$ is the energy consumption weighting coefficient and $W_2$ is the swashplate inclination weighting coefficient.

Constraint 1: Ensure that there is a motor condition in the descending stage, $E_{de} \leq E_{up}$.

Constraint 2: Lifting–lowering–re-lifting time does not exceed a certain value, $t_{tol} \leq t_{up}$.

The single-model parallel optimization mechanism of VAPP's excavator boom energy-recovery system is designed as shown in Figure 19. Due to the high model complexity, running multiple executable programs in parallel can improve simulation efficiency. The parameter-assignment module based on the PSO assigns different parameters to multiple executable programs running at the same time. The parameter-assignment module based on the particle-swarm algorithms reassigns different parameters according to the response and constraints of the objective function. The process of updating the parameters iterates continuously until the decision condition is satisfied.

It is not difficult to find from Figure 20 that along with the increasing iteration times, the fitness value of the optimal objective function and the total energy consumed descended gradually.

Under optimized parameter conditions, the changes of load position and motor energy consumption are shown in Figure 21.

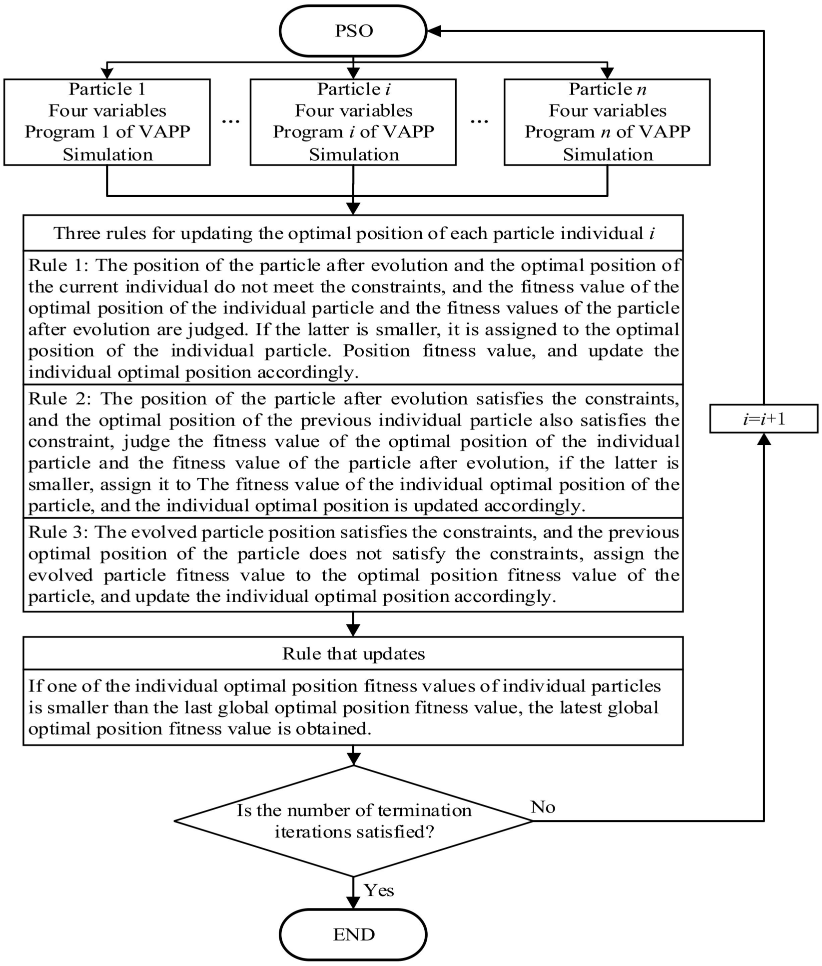


**Figure 19.** Flow chart of PSO.

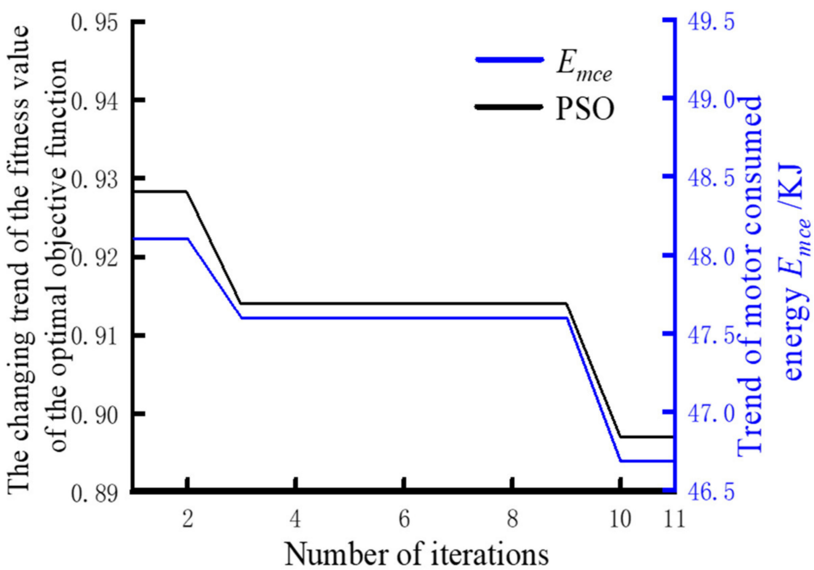


**Figure 20.** The changing trend of the fitness value of the optimal objective function and motor energy consumption.

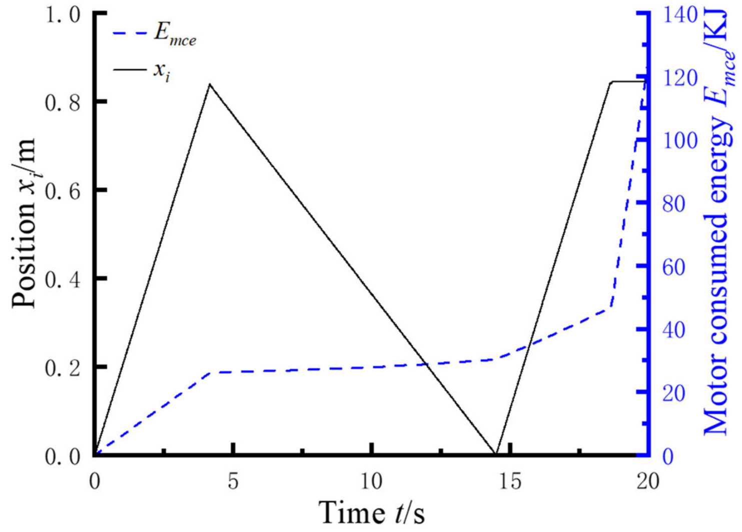


**Figure 21.** Load position and motor energy consumption under optimized parameter conditions.

Table 3 shows the displacement of VAPP and related component parameters required for the optimized 7T-position excavator-boom energy-recovery system.

**Table 3.** The optimized potential-energy-recovery system parameters.

| Displacement of VAPP | The Inclination of Swashplate during Descent | Accumulator Charging Pressure | Accumulator Volume | Energy Consumption |
|---|---|---|---|---|
| 62.47 mL/r | 7.20° | 2.95 MPa | 10 L | 46.7 KJ |

The simulation time comparison is shown in Table 4. It takes 610 min to simulate with SimulationX software, and 55 min to run the CVODE executable. Compared with the SimulationX simulation platform, the efficiency of the .exe simulation program running on an eight-core CPU is increased by more than 80 times.

**Table 4.** Simulation time comparison.

| | SimulationX3.8 | CVODE Executable Program | Multi-Core CPU Parallel Optimization |
|---|---|---|---|
| Total time | 610 min | 55 min | 10 iterations, 10 executable programs in each round, and a total of 100 runs, which takes 720 min. |
| A single time | 610 min | 55 min | 7.2 min |

According to the above method, the simulation of different working conditions is carried out and the appropriate pump displacement (rounded) is selected according to the difference in its minimum equivalent mass. The appropriate swashplate angle is selected in the descending stage, and the appropriate accumulator parameters are selected. Table 5 shows the required pump displacement, the swashplate angle in the descending stage, the initial pressure of the accumulator, the volume parameters of the accumulator, and the energy-saving rate for the 12T, 20T, and 30T excavator booms after optimization.

Under the premise of optimized displacement of VAPP, the influence of the swashplate angle on the energy-saving rate and the completion of the lifting–lowering–re-lifting time of the 12T, 20T, and 30T excavator booms was analyzed, as shown in Figure 22.

**Table 5.** Model parameters.

| Tonnage | 7T | 12T | 20T | 30T |
|---|---|---|---|---|
| Motor speed (rpm) | 2000 | 2000 | 2000 | 2000 |
| Equivalent mass (kg) | 2500 | 3600 | 11,000 | 25,000 |
| Cylinder of Boom—number × cylinder diameter × rod diameter × stroke (mm) | 1 × 110 × 75 × 840 | 1 × 115 × 80 × 1015 | 2 × 120 × 85 × 1290 | 2 × 140 × 100 × 1465 |
| Rated displacement (mL/r) | 65 | 75 | 115 | 160 |
| Swashplate inclination (°) | 7.2° | 7° | 6° | 6° |
| Accumulator pressure P0 (Mpa) | 2.95 | 3.5 | 4.5 | 6.5 |
| Accumulator volume V0 (L) | 10 | 16 | 32 | 50 |
| Energy-saving rate $\eta$ | 29.8% | 35.3% | 31.25% | 27.88% |

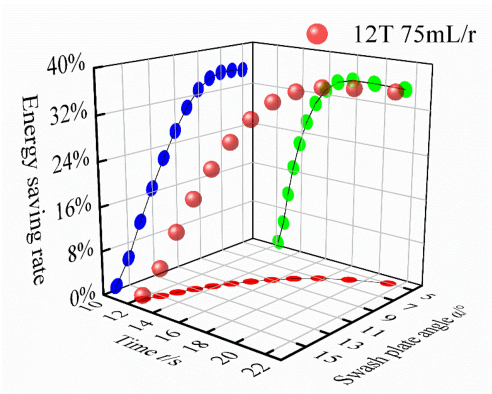


(**a**)

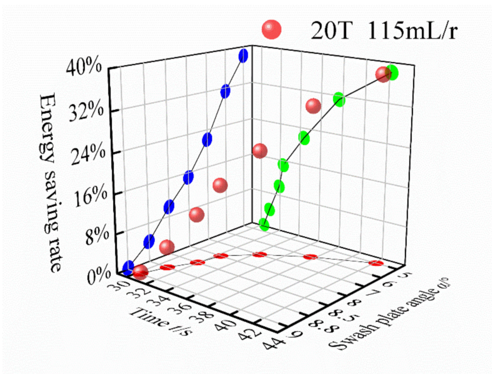


(**b**)

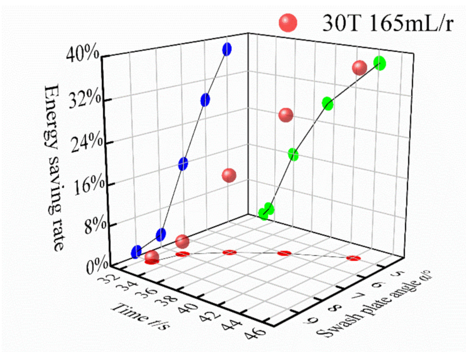


(**c**)

**Figure 22.** Displacement of VAPP and energy-saving rate required for different tons: (**a**) 12T (**b**) 20T (**c**) 30T.

It can be seen from the above figure that the smaller the angle of the swashplate in the descending stage, the easier it is to form the motor working condition, which is beneficial to the recovery of energy. The smaller the swashplate angle, the longer it takes to complete the lift–descent–re-raise. After optimization, it can be concluded that the minimum swashplate angles set by VAPP in the descending stage of the booms of 7T, 12T, 20T, and 30T excavators are: 15.8°, 15.4°, 8.9°, and 8.4°, respectively. When the swashplate angles are less than or equal to these, the excavator boom of each tonnage can achieve energy recovery in the descending stage, and the VAPP must have a motor working condition.

The energy-recovery rate of a common closed-loop boom potential-energy-recovery system is 14.8% [27]. The energy-recovery rate of the optimized closed boom potential-energy-recovery system driven by VAPP is better than that of the ordinary closed boom potential-energy-recovery system.

According to the above-optimized displacement of VAPP required for each tonnage, the relevant values are designed, and the recommended values are given as shown in Table 6.

**Table 6.** VAPP Recommendation Form.

| Tonnage | 7T | 12T | 20T | 30T |
|---|---|---|---|---|
| Rated displacement (mL/r) | 65 | 75 | 115 | 165 |
| Swashplate inclination range (°) | +18~−18 | | | |
| Number of plungers z | 9 | | | |
| Plunger diameter d (mm) | 20 | 21 | 24 | 27 |
| Plunger distribution-circle radius R (mm) | 35.5 | 37.0 | 43.5 | 49.5 |
| Piston stroke (mm) | 23.1 | 24.1 | 28.3 | 32.2 |
| Distribution-groove distribution-circle radius R (mm) | 35.5 | 37.0 | 43.5 | 49.5 |
| The angle of opening of B (°) | 60 | | | |
| The angle of opening of A (°) | 100 | | | |
| The angle of opening of T (°) | 40 | | | |

## 5. Conclusions

Aiming at the problem that parameter matching for VAPP energy-recovery systems for different tonnage excavators is hugely time-consuming and tedious, a rapid multi-process parallel optimization method for complex hydraulic products based on a multi-core CPU was proposed. The solution was designed to ensure that potential energy recovery and utilization could be achieved at any operation condition. The accuracy of the simulation model was verified by a physical prototype test. On this basis, a parameter configuration of boom energy-recovery systems was recommended for conventional 7T, 12T, 20T, and 30T excavators. This is instructive for the design of VAPP serialization excavators. The simulation results show that the energy-saving rate reached 29.8%, 35.3%, 31.25%, and 27.88%, respectively. In addition, the use of this multi-core parallel method can effectively reduce the labor intensity of designers. In the eight-core CPU workstation under the simulation conditions, compared with the Simulation X platform simulation method, the simulation efficiency of the multi-core CPU parallel method was improved by more than 80 times, which has a certain reference value for conventional hydraulic system design.

**Author Contributions:** Y.G. managed the overall conception and theoretical analyses for the paper. L.W. built the simulation model and performed analyses. A.W. derived the equations. Z.N. and L.Q. completed the parameter matching method based on multi-core parallel optimization. All authors have read and agreed to the published version of the manuscript.

**Funding:** This work was supported in part by the National Natural Science Foundation of China under Grant 51875381, in part by the Graduate Innovation Project of Shanxi Province under Grant 2021Y695, in part by the Research Project Supported by Shanxi Scholarship Council of China under Grant 2020-124, and in part by Scientific and Technological Project of Yangquan City under Grant 2022JH053.

**Data Availability Statement:** All data included in this study are available upon request by contacting the corresponding author.

**Conflicts of Interest:** The contact author has declared that neither they nor their co-authors have any competing interest.

## References

1. Andrea, B.; Federico, C.; Mirko, P.; Luca, R.; Paolo, C. Energy saving solutions for a hydraulic excavator. *Energy Procedia* **2017**, *126*, 1099–1106.
2. Guan, D.; Yang, N.; Lai, J.; Siu, M.F.; Jing, X.; Lau, C. Kinematic modeling and constraint analysis for robotic excavator operations in piling construction. *Autom. Constr.* **2021**, *126*, 103666. [CrossRef]
3. Jing, J.; Quan, L.; Huang, J.; Zhao, B. Research on the Characteristics of Asymmetric Pump Directed Controlled Arm Cylinder of Excavator. *J. Mech. Eng.* **2016**, *6*, 188–196. [CrossRef]
4. Lodewyks, J. *Differentialzylinder Im Geschlossenen Hydrostatischen Getriebe*; RWTH Aachen: Aachen, Germany, 1994.
5. Daniel, B.; Claus, H.; Thomas, L. Hybrid-antriebe bei raupenbaggern—Konzepte und losungen. In Proceedings of the 3th Hybridantriebe fur Mobile Arbeitsmaschinen Fachtagung, Karlsruhe, Germany, 17 February 2011; Volume 2, pp. 117–124.
6. Chen, M.; Zhao, D. The gravitational potential energy regeneration system with closed-circuit of boom of hydraulic excavator. *Mech. Syst. Signal Process.* **2017**, *82*, 178–192. [CrossRef]
7. Kilic, E.; Dolen, M.; Caliskan, H.; Koku, A.B.; Balkan, T. Pressure prediction on a variable-speed pump controlled hydraulic system using structured recurrent neural networks. *Control Eng. Pract.* **2014**, *26*, 51–71. [CrossRef]
8. Zhang, S.; Minav, T.; Pietola, M. Improving efficiency of micro excavator with decentralized hydraulics. In Proceedings of the ASME/BATH 2017 Symposium on Fluid Power and Motion Control, Sarasota, FL, USA, 16–19 October 2017; pp. 1–8.
9. Zhang, X.; Quan, L.; Yang, Y.; Wang, C.; Yao, L. Output Characteristics of a Series Three-port Axial Piston Pump. *Chin. J. Mech. Eng.* **2012**, *25*, 498–505. [CrossRef]
10. Hao, Y.; Quan, L.; Cheng, H.; Xia, L.; Ge, L.; Zhao, B. Potential energy directly conversion and utilization methods used for heavy duty lifting machinery. *Energy* **2018**, *155*, 242–251. [CrossRef]
11. Zhang, S.; Jiang, J.; Lian, G. Research on Recoverable Energy Distribution of Hydraulic Excavator. *J. Zhengzhou Univ.* **2014**, *35*, 120–123.
12. Zhang, M.; Wang, Q.; Guan, C. Simulation Research of Parallel Hydraulic Hybrid Excavator. *China Mech. Eng.* **2010**, *16*, 1932–1936.
13. Chen, Q.; Wang, Q.; Wang, T. A novel hybrid control strategy for potential energy regeneration systems of hybrid hydraulic excavators. *Proc. Inst. Mech. Eng. Part I J. Syst. Control Eng.* **2016**, *230*, 375–384. [CrossRef]
14. Qu, W.; Zhou, L.; Zhang, C.; Bo, X. Research Status and Prospect of Hydraulic Energy Storage Technology. *Chin. Hydraul. Pneum.* **2022**, *46*, 93–100.
15. Wang, A.; Lv, Z.; Gao, Y.; Quan, L.; Huang, J. Potential energy recovery scheme with variable displacement asymmetric axial piston pump. *Proc. Inst. Mech. Eng. Part I J. Syst. Control Eng.* **2020**, *234*, 875–887. [CrossRef]
16. Cheng, D.; Gao, Y.; Gong, X.; Li, S. Analysis of energy consumption characteristics of pumping excavator boom based on flow matching. *Mach. Tool Hydraul.* **2019**, *47*, 155–159.
17. Lin, T.; Liu, Q. Method of Parameter Matching for Hydraulic Hybrid System for Excavators. *J. Shanghai Jiao Tong Univ.* **2013**, *5*, 728–733.
18. Xiao, Q. *Control Strategy and Parameter Matching of Hybrid System in Hydraulic Excavator*; Zhejiang University: Hangzhou, China, 2008.
19. Wang, H.; Wang, Q. Parameter Matching and Control of Series Hybrid Hydraulic Excavator Based on Electro-Hydraulic Composite Energy Storage. *IEEE Access* **2020**, *8*, 111899–111912. [CrossRef]
20. Shen, W.; Jiang, J.; Su, X.; Karimi, H.R. Parameter matching analysis of hydraulic hybrid excavators based on dynamic programming algorithm. *J. Appl. Math.* **2013**, *2013*, 1–10. [CrossRef]
21. Lin, X.; Guan, C.; Pan, S.; Wang, D. Parameters matching method for parallel hybrid hydraulic excavators. *J. Agric. Mach.* **2009**, *40*, 28–32.
22. Huang, J.; He, W.; Hao, H. Analysis of Control Characteristics of Variable displacement Asymmetric Axial Piston Pump. *Trans. Chin. Soc. Agric. Mach.* **2019**, *3*, 368–376.
23. Yang, J.; Zhao, B.; Wu, B.; Wang, J.; Lan, Y. Control Performance Analysis of Asymmetric Axial Piston Pump with Variable Displacement. *Chin. Hydraul. Pneum.* **2021**, *2*, 42–49.
24. Xia, L.; Quan, L.; Yang, J.; Zhao, B. Research on the Method of Hydraulic-gas Energy Storage Balancing Hydraulic Excavator Boom Weight. *J. Mech. Eng.* **2018**, *54*, 197–205. [CrossRef]
25. Ning, Z.; Wei, L.; Zhang, R.; Quan, L.; Hua, J.; Gao, Y. Rapid Parallel Optimization Method of Complex Hydraulic Product Based on Multi-core CPU. *Trans. Chin. Soc. Agric. Mach.* **2022**, *53*, 441–449.
26. Wu, T.; Wu, D.; Ren, Y.; Song, Y.; Gu, Y.; Mou, J. Multi-objective optimization on diffuser of multistage centrifugal pump base on ANN-GA. *Struct. Multidisc. Optim.* **2022**, *65*, 182. [CrossRef]
27. Zhao, D.; Chen, M.; Dai, Q.; Zhang, E.; Xu, C. Potential Energy Recovery System for Boom of Hydraulic Hybrid Excavator. *J. Jilin Univ.* **2011**, *41* (Suppl. S1), 150–154.